Performance Evaluation of Masonry Infill Walls in Reinforced Concrete Frames Under Cyclic Loading Using Applied Element Method

Hemanth Kumar Karaka and Rajesh Kumar Tripathi

Abstract Open ground storey in Reinforced concrete framed buildings is considered to be the most vulnerable when it is subjected to dynamic excitation because of the formation of column sway mechanism and then leads to sudden failure of the ground storey. They must be avoided in severe earthquake zones. Many of the researcher's done experiments for the cause of failure in the ground storey and recommended increasing the stiffness and strength in the soft storey for the lateral load resistance by adding a non-structural element such as Masonry infill walls on all sides of the building. It is very complex to study RC frames' behaviour with Masonry infill walls because of different material properties. Numerical tool viz., Finite Element Method used for such complex structural behaviour requires more time for simulation and accuracy is quite acceptable but deviate from the experimental results. For this reason, a powerful numerical tool such as the Applied Element Method (AEM) has been considered. In this paper, one bay-one storey and two bay-two storey half-scale RC frames with and without infill walls under in-plane cyclic loading have been modelled using AEM. In conclusion, the results of AEM models have been compared with experimental results done by researchers. The obtained AEM results are well accepted with experimental results. The study showed that the stiffness, lateral load resistance and strength were improved for masonry infilled RC frame, compared with bare RC frame in both Single-storey and Multi-storied frames.

Keywords Applied element method · Displacement controlled cyclic loading · Lateral load resistance · Displacement ductility factor · Displacement ductility · Cracked stiffness

H. K. Karaka (✉) · R. K. Tripathi
Department of Civil Engineering, National Institute of Technology Raipur, Raipur, Chhattisgarh, India
e-mail: khkumar.phd2019.ce@nitrr.ac.in

R. K. Tripathi
e-mail: rktripathi.ce@nitrr.ac.in

G. C. Marano et al. (eds.), *Proceedings of SECON'21*, Lecture Notes in Civil Engineering 171, https://doi.org/10.1007/978-3-030-80312-4_80

1 Introduction

Analytically, the masonry structure behaviour is quite complex because of the heterogeneity in construction. Several numerical modelling techniques were developed to study the crack patterns in masonry walls. There are several limitations in numerical methods to approximate the behaviour of the infilled wall structure. Several numerical procedures were adapted to reduce approximation levels. In this context, the most popular method, i.e., the Finite Element Method (FEM), implemented for the masonry structures and constitutive laws for nonlinear behaviour in account with the material homogenisation process. Continuum idealisation, or macro-modelling, and system discontinuity, or micro-modelling, are two numerical approaches that are mainly used. In Roca et al. [1], the overview of these methods has been presented. Although, there are several extensions and hybrid methods developed for FEM, it is very difficult to achieve the element separation, rotation. The formulation for the distinct nature of masonry was started in the early seventies [2]. In the Discrete Element Method (DEM), the elements that can be modelled as rigid, partial-rigid, or deformable were considered. Unlike FEM, DEM elements remeshing is not required at the stress concentration region [3]. Cundall and Hart [4], the classical DEM have two main hypotheses, i.e. Element finite displacement and rotations, element contact or collision. In Lourenço [5], recent improvements of various methods such as MDEM, EDEM, DEM compared with FEM were depicted. The collapse behaviour of structures can be achieved in DEM. Because of this feature, many DEM related applications were developed. However, attaining real collapse behaviour of structures is difficult because inefficiency of damping factors. The examples of successful applications of DEM for earthquake analysis of masonry structures were well presented [6, 7] in their research.

Recently the Non-Smooth Contact Dynamics method adapted for the masonry structures under in-plane dynamic loading to study the behaviour [8, 9].

The rigid body spring model (RBSM) [10] partially overcome these issues in DEM. In this method, a masonry elements assembly is assumed as rigid elements connected with normal and shear springs. The structural response can be achieved by the deformation of springs. Although RBSM is well handed for static problems, dynamic analysis can also be applied; under several assumptions, adequate results can be obtained.

Meguro and Tagel-Din [11] came with a similar approach named as Applied Element Method (AEM), in which rigid elements connected by material springs. The stiffness of the springs in both normal and shear directions need to be calculated for the material behaviour. In the AEM [12], analysis can be carried out until the complete collapse of a structure. In RBSM, it is not possible to follow the complete collapse behaviour of the structure.

In the current research, Single-storey and Multi-storey RC bare frames with masonry infill walls were considered to study the behaviour of structures using the AEM.

2 Discretisation of Masonry Elements in Applied Element Method

According to Malomo [13], assembly by zero thickness springs of masonry elements as rigid units. In between the masonry elements, unit interface mortar properties are lumped. The simplified micro-modelling strategy of masonry with mortar shown in Fig. 1a.

The arrangement of interface springs and unit springs in series, stiffness k_{ni} and k_{si} shown in Eq. (1). k_{nu} and k_{su}, are unit deformation stiffnesses of springs connected between the masonry elements as shown in Eq. (2),

$$k_{nu} = \left(\frac{l_i - t_{mo}}{E_u dt_u} + \frac{t_{mo}}{E_{mo} dt_u}\right)^{-1}, \quad k_{su} = \left(\frac{l_i - t_{mo}}{G_u dt_u} + \frac{t_{mo}}{G_{mo} dt_u}\right)^{-1} \tag{1}$$

$$k_{ni} = \frac{E_u - dt_u}{l_u}, \quad k_{si} = \frac{G_u - dt_u}{l_u} \tag{2}$$

where l_i is the distance between the centroidal nodes of interface elements, l_u is the distance between the centroidal nodes of masonry elements, t_{mo} is the mortor bond thickness, t_u is the unit thickness of mortor, d is spacing of transverse springs, and E_u, E_{mo} are Young's modulus of unit mortar and actual mortar respectively, G_u and G_{mo} are Rigidity modulus of unit mortar and actual mortar, respectively.

3 Experimental Data

Ahmed Sayed [14] was conducted the experimental work on four half scaled Single-storey Reinforced Concrete frame specimens such as bare frame, hollow red brick infill wall of thickness 120 mm, hollow red brick infill wall of thickness of

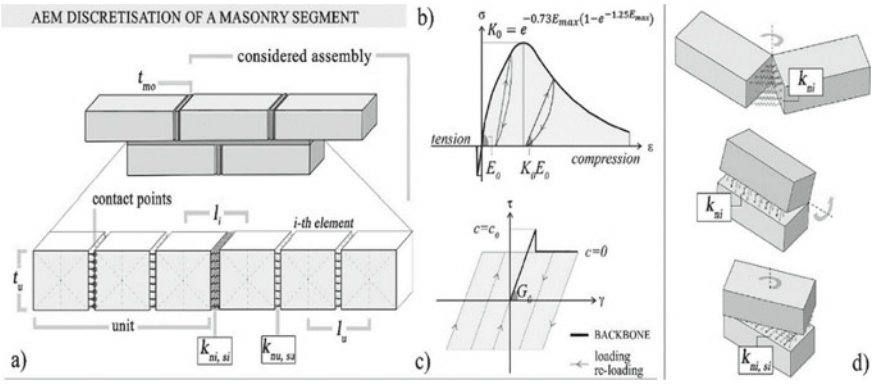

Fig. 1 Masonry assembly in AEM: **a** AEM discretisation of masonry elements, **b** σ-ε relationship of normal springs, and **c** σ-ε relationship of shear springs in cyclic loading, **d** bending and twisting of elements [13]

60 mm and cement bricks infill wall of thickness 120 mm. From his study, it was concluded that the lateral load resistance of the frame with second specimen i.e., holes red bricks masonry of thickness 120 mm was 184% greater than the first specimen i.e., bare frame, whereas for the third and fourth specimen are by 61% and 99% respectively. The initial stiffness of the second specimen is much greater than the remaining specimens.

For this reason, the current research has chosen hollow red brick infill walls of 120 mm thick to study the behaviour of two-storey two-bay RC frame with and without infill walls subjected to in-plane cyclic loading using the Applied Element Method.

4 Modelling of RC Frames

Five half scaled Reinforced Concrete models, namely SBF1, SIF1, MBF, MSF, MIF shown in Fig. 2. were considered for the nonlinear behaviour under cyclic load analysis using Applied Element Method. The first two RC models, i.e., SBF1 & SIF1 details, were taken from Ahmed Sayed's experimental work [14], namely SBF2 & SIF2, to validate numerical models. The Single-storey and Multi-storey RC bare frames were considered for infill wall models also.

5 Sectional & Reinforcement Details

The beams of cross-section 120 × 200 mm, columns of cross-section 200 × 120 mm and base of cross-section 300 × 500 mm are considered. Hollow Red Bricks of size 215 × 102.5 × 65 mm is used for masonry infill wall. High yield strength deformation bars as main reinforcement and Mild steel bars as shear reinforcement are considered. The sectional and reinforcement details of all models are shown in Table 1.

6 Material Properties

High Strength Concrete (HSC) is considered for beams and columns, and Normal Strength Concrete for Base is considered for all the models. Hollow Red Bricks is considered for Masonry infill wall (Table 2).

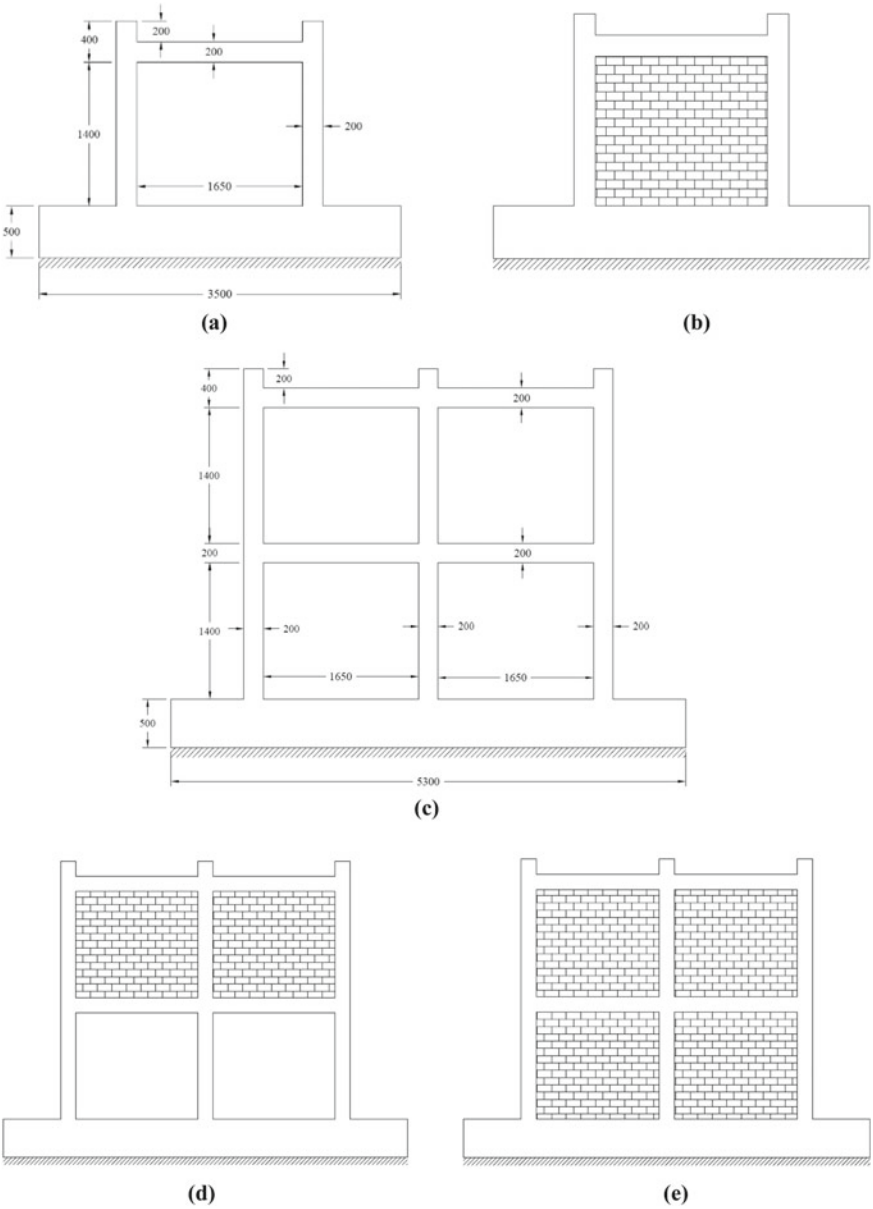

Fig. 2 Elevation of models: **a** single-storey bare frame—SBF1 & SBF2, **b** single-storey infill frame—SIF1 & SIF2; **c** multi-storey bare frame—MBF, **d** multi-storey soft-storey frame—MSF, **e** multi-storey infill frame—MIF

Table 1 Sectional and reinforcement details of all models

Name of the specimen	Member	Cross-sectional area (mm^2)	Reinforcement details
	Base	300 × 500	4–12 mmφ (top and bottom) 8 mmφ @ 180 mm c/c (stirrups)
SBF1, SIF1, MBF, MSF, MIF	Beam	120 × 200	2–12 mmφ (top and bottom) 8 mmφ @ 154 mm c/c (stirrups)
	Column	200 × 120	2–12mmφ (top and bottom) 8 mmφ @ 140 mm c/c (stirrups)

Table 2 Material properties of SBF1, SIF1, MBF, MSF, MIF [14]

Material properties	High strength concrete	Normal strength concrete	Steel	Hollow red brick
Compressive strength, GPa	0.065	0.03	0.42	0.004
Tensile strength, GPa	0.007	0.003	0.42	0.0004
Young's modulus, GPa	41.8	25	214.2	4.6
Shear modulus, GPa	17.5	11	82.6	1.8
Strain separation	0.1	0.1	0.15	0.1
Frictional coefficient	0.8	0.8	0.8	0.8
Specific weight, kg/m^3	2,750	2,500	7,850	1,635
Peak stress/yield tensile stress	–	–	1.39	–
The ratio of post-yield stiffness	–	–	0.01	–

7 Loading Configuration

All the models were subjected to cyclic displacement controlled loading condition, as shown in Fig. 3. The displacement history was the same for all tested models; Incremental Displacement considered in five stages viz., Stage 1: ±0.5 mm until 3 mm, Stage 2: ±1.0 mm until 10 mm, Stage 3: ±2.0 mm until 20 mm, Stage 4: ±4.0 mm until 40 mm, and Stage 5: ±10.0 mm up to 100 mm.

8 Results and Discussions

8.1 Mode of Failure

For frame SBF1, hair cracks observed in the columns at beam-column juncture at the end of cycle 2 mm, but for SBF2, it was observed at cycle −2 mm. The cracks were closed and opened for the increased in-plane load for each cycle. Upon application of repeated cyclic load, the flexural and shear compression cracks

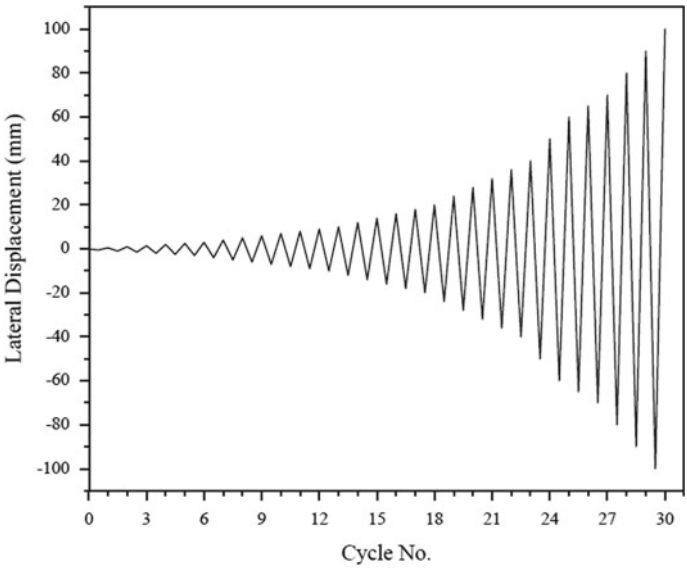

Fig. 3 Displacement history considered for all the models

observed at one-fourth of the column base and beam-column connection, respectively. At higher amplitudes of repeated cyclic load, diagonal cracks initiated and large crack openings can be seen at the beam-column junction after cycle +50 mm. The point of failure observed at +61.28 mm.

For frame SIF1, minor cracks observed in the masonry wall diagonally at the end of cycle −2 mm, but for SBF2, it was observed at cycle −1.5 mm. The cracks were closed and opened for the increased in-plane load for each cycle. Upon application of repeated cyclic load, diagonal crack further extended, and the brick element starts separating from each other at the centre at low-level loading. Lateral strength improved when compared with SBF1 but failed at cycle +12 mm. The Ultimate lateral load and Relative Displacement of SBF1, SBF2, SIF1, SIF2 shown in Table 3.

The mode of failure of SIF1 and SIF2 almost matching each other to the maximum extent.

Table 3 Numerical and experiment comparision of ultimate lateral load and relative displacement of single-storey bare frame and infill frame specimens

Specimen	SBF1	SBF2	SIF1	SIF2
	numerical	experiment	numerical	experiment
Ultimate lateral load (ton)	6.97	6.63	18.44	18.098
Relative displacement (mm)	61.58	60.32	12.195	12.06

From Table 3 and Fig. 4, it was observed that the AEM results were well accepted with experimental results. Further, the displacement controlled load condition is applied to MBF, MSF, MIF to study the behaviour.

From Table 4, the Ultimate lateral load of MSF is more compared with MIF has been observed. It is because of the weak column and strong infill wall.

From Table 4,

- For frame SIF1, the ultimate in-plane load resistance is 164% more, compared with the frame SBF1
- For frame MSF, the ultimate in-plane load resistance is 411% more, compared with the frame MBF
- For frame MIF, the ultimate in-plane load resistance is 396% more, compared with the frame MBF

The shear failure observed at the base of either side column for MSF, whereas for MIF, the flexural failure observed at the beam-column juncture of either side columns of the first floor and shear failure observed at the base of the middle column.

Fig. 4 Mode of failure of: **a** experimental infill frame (SIF2) [14] and **b** numerical infill frame (SIF1)

Table 4 Relative displacement and ultimate in-plane load of all models

Specimen	Relative displacement (mm)	Ultimate in-plane load (ton)
SBF1	61.58	6.97
SIF1	12.195	18.44
MBF	44.90	14.70
MSF	24.06	60.44
MIF	20.23	58.23

8.2 Relationship Between In-Plane Load and Displacement

Plots of the hysteresis envelope of lateral load versus lateral displacement till the collapse of all the specimens shown in Fig. 5. The plots show the behaviour of all the specimens from the elastic stage to the collapse stage.

8.3 Ductility

According to Comite Euro-International Du Beton, 1996 [14], the Displacement ductility factor (Rμ) is the ratio between displacement at failure point (Δ_f) to displacement at the yield point of the specimen (Δ_y) shown in Eq. (3) and the Displacement Ductility is the ratio of maximum displacement in each cycle interval (Δ_i) to the displacement at the yield point (Δ_y) shown in Eq. (4) where these displacements are obtained from the plot of lateral force and lateral displacement of the specimen. The yield displacement is 80% of the ultimate load on the rising curve of lateral load versus lateral displacement plot of the specimen. The failure displacement is 80% of the ultimate load on the falling curve of load versus the displacement plot of the specimen.

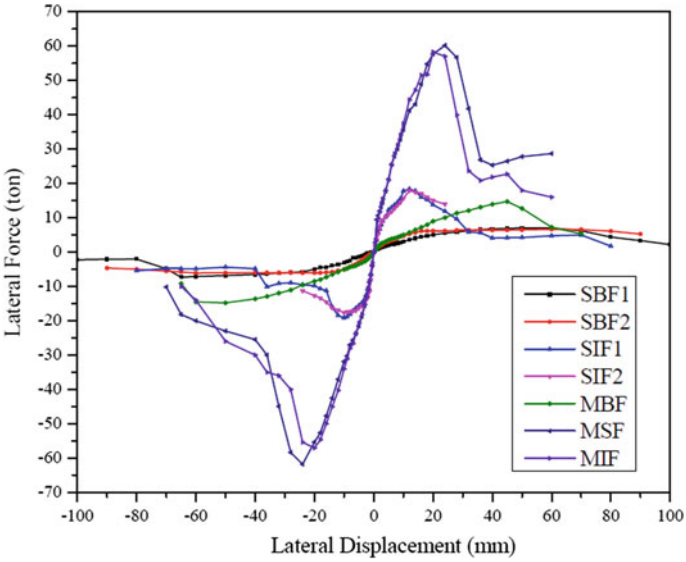

Fig. 5 Hysteresis envelope of all the specimens till the collapse

Table 5 Accumulated displacement ductility and displacement ductility factor Rμ

Specimen	Accumulated displacement ductility	Displacement ductility factor, Rμ
SBF1	23.53	2.71
SIF1	7.81	1.17
MBF	14.753	2.05
MSF	12.86	1.90
MIF	13.01	1.93

$$\text{Displacement ductility factor}, R\mu = \frac{\Delta_f}{\Delta_y} \tag{3}$$

$$\text{Displacement Ductility} = \frac{\Delta_i}{\Delta_y} \tag{4}$$

where Δ_f is the displacement at failure point, Δ_y is the displacement at the yield point, Δ_i is the maximum displacement in each cycle interval.

The Accumulated Displacement Ductility is the accumulation of the lateral displacement of first cycle until the failure load cycle and expressed by Eq. (5).

$$\text{Accumulated Displacement Ductility} = \sum \left(\frac{\Delta_i}{\Delta_y}\right) \tag{5}$$

From Table 5,

- For frame SIF1, the accumulated displacement ductility is 67% lesser than that of frame SBF1
- For frame MSF, the accumulated displacement ductility is 13% lesser than that of frame MBF and also 1.15% lesser than of frame MIF
- For frame MIF, the accumulated displacement ductility is 12% lesser than that of frame MBF but 1.16% greater than of frame MSF

8.4 Stiffness

According to Comite Euro-International Du Beton, 1996 [14], the stiffness of structure can be computed for the each interval of cyclic loading as the ratio of peak load at a particular cycle to the peak displacement of the same cycle.

$$\text{Cracked Stiffness}, k_i = \frac{P_i}{\Delta_i} \tag{6}$$

where, P_i is the peak load at cycle i, Δ_i is the peak displacement at cycle i (Fig. 6).

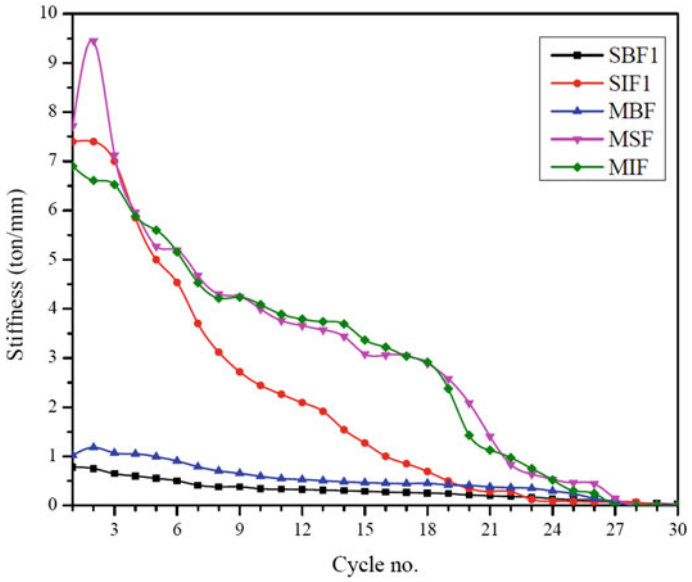

Fig. 6 Stiffness degradation versus the number of cycles

Table 6 Initial stiffness (ton/mm) of all models

Model	Initial stiffness (ton/mm)
SBF1	0.552
SIF1	2.74
MBF	0.903
MSF	3.99
MIF	4.087

The initial stiffness is the ratio of change in lateral load to change in lateral displacement for the tangent drawn at the 5th cycle. Table 6 shows the initial stiffness for all models.

From Table 6,

- For frame SIF1, the initial stiffness is 396% greater than that of frame SBF1
- For frame MSF, the initial stiffness is 341% greater than that of frame MBF
- For frame MIF, the initial stiffness is 352% greater than that of frame MBF

9 Conclusions

From this study, it can be concluded that;

1. Applied Element Method results are well accepted with experimental results.
2. The Displacement Ductility Factor of bare frames is greater than the infill frames in both Single-storey and Multi-storey frames i.e., SBF1 = 2.71, SIF1 = 1.17, MBF = 2.05, MSF = 1.90, and MIF = 1.93.
3. The accumulated displacement ductility for SIF1 with an infill wall of thickness 120 mm was less than the bare frame SBF1 by about 67%. The accumulated displacement ductility of frames MSF and MIF with infill walls is less than bare frame MBF by about 13% and 12% respectively.
4. The strength of frame SIF1 with an infill wall was 164% stronger than the bare frame SBF1. The strength of frames MSF and MIF with infill wall of 411% and 396% respectively were stronger than the bare frame MBF.
5. The ultimate in-plane load resistance for frame MSF was greater than the frame MIF by about 3.79% because of the weak column, strong infill wall behaviour.
6. The shear failure observed at the base of either side columns for MSF, whereas for MIF, the flexural failure observed at the beam-column juncture of either side columns of the first floor and shear failure observed at the base of the middle column.
7. Stiffness degradation of masonry infilled frames is very rapid compared to bare frames. Whereas the initial stiffness of SIF1 is 396% greater than that of frame SBF1 and the initial stiffness of MSF and MIF is greater than MBF by about 341% and 352%, respectively.

Acknowledgements The authors warmly acknowledge the support of Ministry of Human Resources and Development (MHRD), India and N.I.T Raipur for providing continuous support.

References

1. Roca P, Cervera M, Gariup G, Pela' L (2010) Structural analysis of masonry historical constructions. Classical and advanced approaches. Arch Comput Methods Eng 17:299–325. https://doi.org/10.1007/s11831-010-9046-1
2. Cundall AP (1971) A computer model for simulating progressive, large-scale movement in blocky rock system. Proc Int Symp Rock Mech
3. Lemos JV (2007) Discrete element modeling of masonry structures. Int J Archit Herit 1:190–213. https://doi.org/10.1080/15583050601176868
4. Cundall PA, Hart RD (1992) Numerical modelling of discontinua. Eng Comput 9:101–113. https://doi.org/10.1108/eb023851
5. Lourenço PB (2002) Computations on historic masonry structures. Prog Struct Eng Mater 4:301–319. https://doi.org/10.1002/pse.120
6. De Lorenzis L, DeJong M, Ochsendorf J (2007) Failure of masonry arches under impulse base motion. Earthq Eng Struct Dyn 36:2119–2136. https://doi.org/10.1002/eqe.719

7. Tondelli M, Beyer K, DeJong M (2016) Influence of boundary conditions on the out-of-plane response of brick masonry walls in buildings with RC slabs. Earthq Eng Struct Dyn 45:1337–1356. https://doi.org/10.1002/eqe.2710
8. Chetouane B, Dubois F, Vinches M, Bohatier C (2005) NSCD discrete element method for modelling masonry structures. Int J Numer Methods Eng 64:65–94. https://doi.org/10.1002/nme.1358
9. Meguro K, Tagel-Din H (2002) Applied element method used for large displacement structural analysis. J Nat Dis Sci 24:25–34
10. Kikuchi A, Kawai T, Suzuki N (1992) The rigid bodies-spring models and their applications to three-dimensional crack problems. Comput Struct 44:469–480. https://doi.org/10.1016/0045-7949(92)90269-6
11. Meguro K, Tagel-Din H (2000) Applied element method for structural analysis: theory and application for linear materials. Struct Eng Eng 17. https://doi.org/10.2208/jscej.2000.647_31
12. Karbassi A, Nollet MJ (2013) Performance-based seismic vulnerability evaluation of masonry buildings using applied element method in a nonlinear dynamic-based analytical procedure. Earthq Spectra 29:399–426. https://doi.org/10.1193/1.4000148
13. Malomo D, Pinho R, Penna A (2020) Numerical modelling of the out-of-plane response of full-scale brick masonry prototypes subjected to incremental dynamic shake-table tests. Eng Struct 209:110298. https://doi.org/10.1016/j.engstruct.2020.110298
14. Tawfik Essa ASA, Kotp Badr MR, El-Zanaty AH (2014) Effect of infill wall on the ductility and behavior of high strength reinforced concrete frames. HBRC J 10:258–264. https://doi.org/10.1016/j.hbrcj.2013.12.005